Available online at www.sciencedirect.com
SCIENCE DIRECT®
Ocean Modelling 12 (2006) 1–15
Ocean Modelling
www.elsevier.com/locate/ocemod

Rediscovering the second core of the Atlantic NECC

D.F. Urbano [a], M. Jochum [b,*], I.C.A. da Silveira [a]

[a] *Universidade de São Paulo, Instituto Oceanográfico, Departamento de Oceanografia Física, Química e Geológica, São Paulo 05508-900, SP, Brazil*
[b] *National Center for Atmospheric Research, Oceanography Section, Room 415, P.O. Box 3000, Boulder, CO 80307-3000, USA*

Received 11 January 2005; received in revised form 21 March 2005; accepted 12 April 2005
Available online 13 June 2005

Abstract

The North Equatorial Countercurrent (NECC) is investigated at 35°W through a combination of theory, high resolution Ocean General Circulation Model outputs, and observations. Transport from ADCP measurements during four WOCE cruises and from 5-year SeaWinds scatterometer wind data (QuikSCAT satellite) were used to support model results. It is found that the NECC in the annual mean is approximately in Sverdrup balance, but that seasonal changes in the wind stress curl lead the transport expected from the Sverdrup balance by one month, the propagation time of the seasonal Rossby waves from the African coast to 35°W. An investigation of the vertical structure of the NECC shows that there is an eastward core throughout the year, but in spring it is below the westward Ekman flow. Only 60% of the total transport are above the thermocline. The most interesting result of the present study is that model as well as observations describe a distinct second, northern core of the NECC which has not yet found much attention in the literature. It is shown here that the two cores of the NECC are the direct result of the finite width of the Inter-tropical Convergence Zone (ITCZ). This suggests that observational programs that try to determine the NECC transport have to cover the area up to 15°N.
© 2005 Elsevier Ltd. All rights reserved.

Keywords: NECC; Sverdrup; Tropical Atlantic; ITCZ

* Corresponding author. Tel.: +1 303 497 1743.
E-mail addresses: dfurbano@io.usp.br (D.F. Urbano), markus@ucar.edu (M. Jochum), ilson@io.usp.br (I.C.A. da Silveira).

1463-5003/$ - see front matter © 2005 Elsevier Ltd. All rights reserved.
doi:10.1016/j.ocemod.2005.04.003

1. Introduction

In the equatorial zone, separating the oppositely rotating North and South Atlantic gyres, a dynamically complex system of currents flows mainly in the zonal direction. The westward North and South Equatorial Currents (NEC and SEC), which are the equatorward arms of the subtropical gyres, are separated by the North Equatorial Countercurrent (NECC) and the Equatorial Undercurrent (EUC), both flowing east. This zonal current system is an important dynamical feature in the central part of the tropical Atlantic Ocean and plays a fundamental role in its mass and heat budget.

Based on historical hydrographic sections, Garzoli and Katz (1983) studied the NECC and its relation to the seasonal varying winds from 48°W to 10°W. Through the analysis of the shallow water vorticity equation, they showed that Ekman pumping and divergence of geostrophic currents are the dominant forces between 42°W and 22°W; thus, the NECC is in Sverdrup balance there. West of 42°W, this balance breaks down, either because of friction or nonlinearity; the data did not permit to resolve this issue. Their results also suggest a one to two month lag between the curl of the wind stress and thermocline displacement.

Following Garzoli and Katz (1983), Verdy and Jochum (2005) applied numerical modeling to determine the complete annual mean vorticity balance in the western part of the basin which is not in Sverdrup balance. They showed that the nonlinear advective terms account almost entirely for the departures from Sverdrup balance.

The purpose of the present work is to combine theory with outputs of a high resolution Ocean General Circulation Model (OGCM) and observational data at 35°W to better understand the seasonal cycle and the spatial structure of the NECC. Model outputs are mainly necessary to supply missing information in the measured field and also provide a synoptic view of the local dynamics.

Surprisingly, the model revealed that the NECC consists of two separate cores throughout most of the year. The existence of the second core in the real ocean could be verified by revisiting observational descriptions of the NECC. While we found many studies that indicate the existence of the second, northern core, only two studies explicitly mention it: Schott and Böning (1991) find it as a numerical solution for the Atlantic circulation, and Didden and Schott (1992) described it during the analysis of Geosat altimetry. The first of these studies suggests that the second core is dependent on the details of the vertical viscosity, but a dynamical explanation for the second core has not been attempted in either of these studies. Since most observational programs since then do not cover the area of the northern core, we speculate that the second has since been forgotten or not deemed worthy of investigation. Here we show, however, that the second core is a beautiful example for the explanatory power of the Sverdrup balance.

The model configuration is briefly described in Section 2. The data used here to validate model results are presented in Section 3. The structure of the NECC is described in Section 4. Section 5 discuss the results, and Section 6 summarizes them.

2. Theory and model description

The connection between then oceanic interior flow and the wind field was described by Sverdrup (1947). Neglecting nonlinear and non-stationary terms as well as interior friction, the meridional transport in the ocean can be estimated from the curl of the wind stress alone

$$\beta V = \hat{k} \cdot \nabla \times \tau, \tag{1}$$

where β is the y-derivative of the Coriolis parameter; V represents the meridional depth-integrated transport from surface to bottom; and τ is the wind stress. The Sverdrup transport accounts for the transport within the Ekman layer plus the geostrophic transport.

The total field of Sverdrup transport can be computed using a stream function

$$U = -\frac{\partial \Psi}{\partial y}, \tag{2}$$

$$V = \frac{\partial \Psi}{\partial x}, \tag{3}$$

that applied to Eq. (1) gives

$$\beta \Psi(x, y) = \int_{x_0}^{x} (\hat{k} \cdot \nabla \times \tau)\, \mathrm{d}x + F(y). \tag{4}$$

To assure that there is no flow into the wall in the boundary $x = L$, the integration constant $F(y)$ can be specified by

$$F(y) = -\int_{x_0}^{L} (\hat{k} \cdot \nabla \times \tau)\, \mathrm{d}x, \tag{5}$$

where x_0 is Africa's coast and L for the present purpose is 35°W.

Applying Eq. (2) into Eq. (4), the zonal Sverdrup transport is computed by

$$U = -\frac{1}{\beta}\left(\int_{x_0}^{x} \frac{\partial(\hat{k} \cdot \nabla \times \tau)}{\partial y}\, \mathrm{d}x - \int_{x_0}^{L} \frac{\partial(\hat{k} \cdot \nabla \times \tau)}{\partial y}\, \mathrm{d}x\right). \tag{6}$$

For the sake of simplicity we will use the term Sverdrup transport for both the meridional and the zonal transports as defined above. Because of the strong variability in the tropics, observations alone are not sufficient to cover all regions between Africa and South America nor can they explain the dynamics in a synoptic framework. Thus model results are useful to link theory and observations resulting in a consistent interpretation of the equatorial dynamics.

The outputs of the Modular Ocean Model 2b, earlier applied to study the Atlantic western boundary processes in the NBC region (Jochum and Malanotte-Rizzoli, 2003), are used here. The model configuration is an idealized basin from 25°S to 30°N in latitude and from 70°W to 15°E in longitude, with a flat bottom at 3000 m. The resolution is 1/4° by 1/4° at the western boundary between the equator and 12°N, becoming coarser toward the eastern, northern and southern boundaries (Fig. 1(a)). Thirty levels are used in the vertical, with 10 m resolution in the first 100 m. The initial condition is a state of rest. Salinity is kept constant in time and space at a value of 35 psu. The initial temperature distribution is symmetric about the equator and is basically a zonally averaged idealized climatology (Liu and Philander, 1995). Horizontal mixing is done by a Laplacian scheme with the eddy viscosity and diffusivity being linearly dependent on the resolution: from 200 $m^2\ s^{-1}$ for 1/4° to 2000 $m^2\ s^{-1}$ for 1° resolution. In the vertical, a Richardson number-dependent vertical mixing scheme is used. Unstable temperature gradients are eliminated by mixing heat vertically to a depth that ensures a stable density gradient. The warm

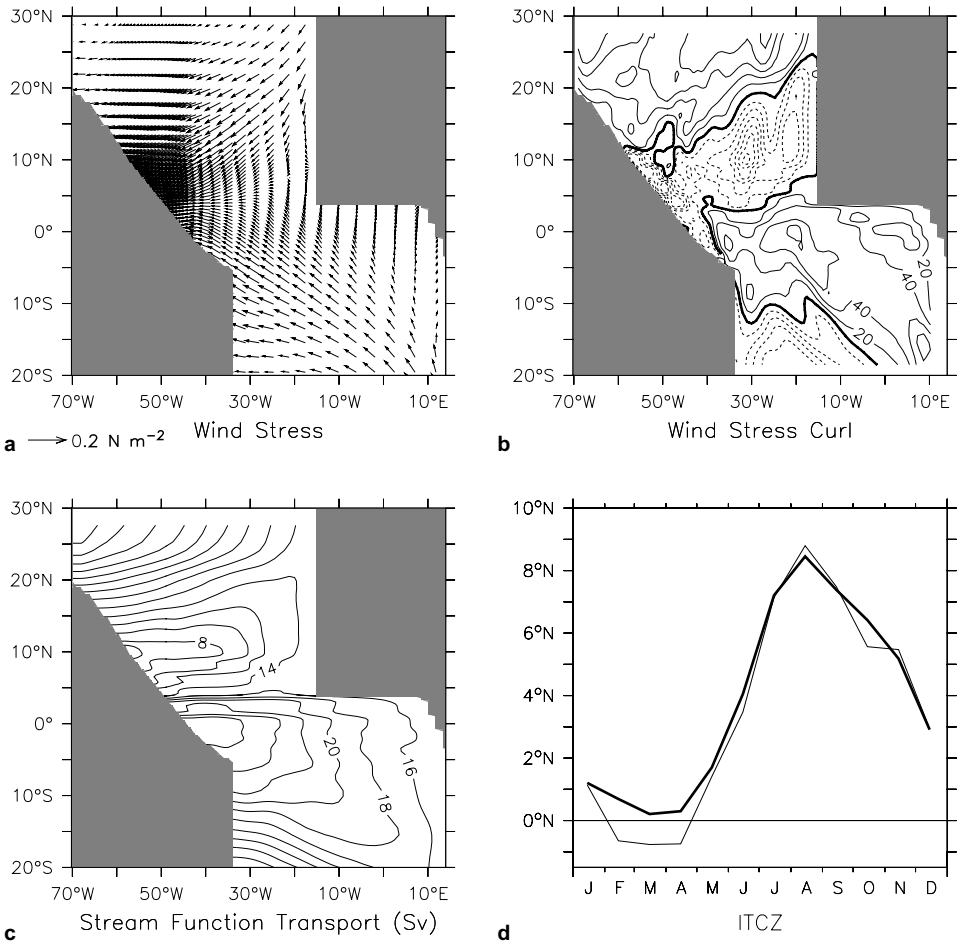

Fig. 1. The South American and African idealized continents are shown in gray. (a) Horizontal map of annual wind stress in N m^{-2}. (b) Annual mean of the wind stress curl ($\times 10^{-9}$ kg s^{-2}). (c) Annual mean stream function transport Ψ in Sv. The contour interval is 2 Sv. (d) Position of the most equatorward zero wind stress curl line through the year for 35°W (thin line) and the zonal mean for all grid points between 35°W and 25°W (thick line).

water path of the meridional overturning circulation is accounted for by open boundary conditions: throughout the year, 15 Sv of water enter the basin above the thermocline across the southern boundary and leave it again at the northwestern corner (Fig. 1(c)). The monthly mean climatological wind stress (Hellerman and Rosenstein, 1983) interpolated to the model grid is shown in Fig. 1(a). The model is spun up for 20 years and the presented results are taken from the following four years of model integration. The stream function transport computed using Eq. (4) is shown in Fig. 1(c). A series of detailed comparisons between observations and the model results demonstrates that the present setup, although idealized, is able to reproduce the North Brazil Current (NBC), the NBC rings (Jochum and Malanotte-Rizzoli, 2003), tropical instability waves (Jochum et al., 2004) and the NECC at 38°W (Verdy and Jochum, 2005).

The tropical Atlantic circulation and in particular the NECC exhibits a strong seasonal cycle forced by the migration of the Inter-tropical Convergence Zone (ITCZ) (Katz and Garzoli, 1982; Katz, 1987; Garzoli and Richardson, 1989; Garzoli, 1992). Fig. 1(b) and (d) show the annual mean of the wind stress curl and the ITCZ position, respectively. The seasonal cycle of the ITCZ position was computed as the most equatorward position of the zero wind stress curl for 35°W (thin line), and for the mean of all grid points between 25°W and 35°W (thick line).

3. Observations

Two sets of high resolution data are used here to support the model results: in situ velocity measured by Acoustic Doppler Current Profiler (ADCP), and surface velocity wind obtained by satellite scatterometer.

Direct velocity measurements in the NECC region are still few since most of the recent observational programs do not reach latitudes higher than few degrees north. For example, Schott et al. (1998) discuss in detail the transports and pathways in the western tropical Atlantic using hydrography, current profiling and moorings, but the NECC was not covered at 35°W due to lack of observations north of 4°N. However, as a part of WOCE four cruises provided ADCP data up to 7.5°N: CITHER1, ETAMBOT2, EQUALANT99, and ETAMBOT1. The full data sets description were presented by Arhan et al. (1998) and Bourlès et al. (1999a, 2002). Since the goal here is only to validate the model results, we restricted ourselves to direct velocity measurements, thus avoiding the uncertainties arising from the level-of-no-motion problem.

The SeaWinds scatterometer onboard of the QuikSCAT satellite has been successfully collecting data since 1999 (Liu, 2002). A 5-year monthly averaged wind climatology was built for the time from September 1999 to August 2004. The wind stress components were calculated using the bulk formula

$$(\tau^x, \tau^y) = \rho_a C_D |\vec{V}|(u, v), \tag{7}$$

where τ^x and τ^y are the zonal and meridional wind stress components, ρ_a is the density of air (1.3 kg m^{-3}), $|\vec{V}|$ is the wind speed, u and v are the zonal and meridional wind components, respectively, and C_D is the drag coefficient calculated according to Large and Pond (1981).

4. Description of the model NECC

Seasonal maps of model zonal velocity at 35°W were constructed for the first 400 m, with the isotherm of 21.5 °C superimposed on the velocity contours to represent the thermocline (Fig. 2). This value was chosen based on the maximum vertical gradient of temperature.

Above the thermocline, the NECC extends from 3°N to 13°N and consists of *two* separate cores that move toward and away from each other over the course of the year. The southern NECC branch (sNECC) is centered near 6°N during most of the year, but has its southernmost position during the summer. The northern branch (nNECC) and the sNECC are both stronger in the second half of the year.

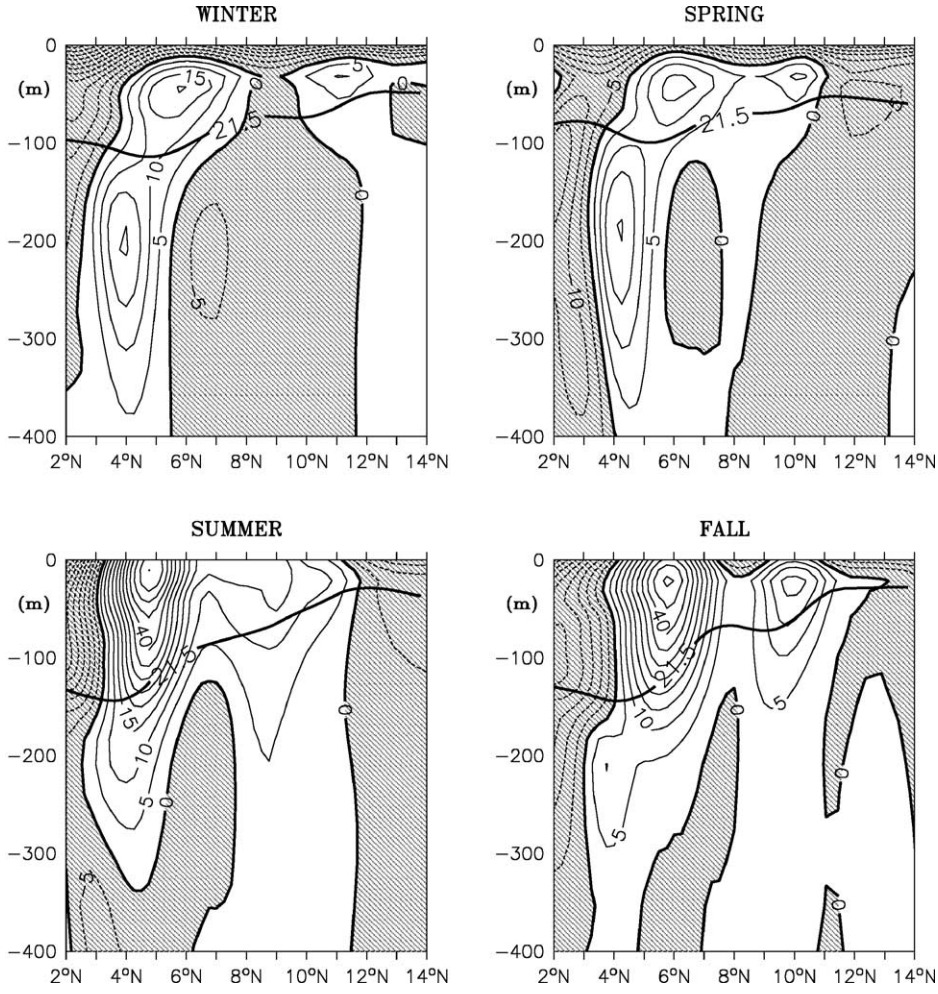

Fig. 2. Seasonal sections of model zonal velocity at 35°W. The contour interval is 5 cm s^{-1}, and dashed lines represent negative (westward) velocities. The isotherm of 21.5 °C was overlaid and represents the thermocline surface.

The seasonal variability of the core position is slightly larger for the nNECC than for the sNECC, varying between 11°N in the winter and 9°N in the summer. The two branches are completely separated by westward flow during the winter but connected for the rest of the year.

Below the thermocline between 2°N and 6°N at 200 m depth is the North Equatorial Undercurrent (NEUC), which is connected with the sNECC throughout the year. During the summer, the NECC's 20 cm s^{-1} isotach makes the core structure of the NEUC disappear; the NEUC is no longer centered at 200 m and appears to be almost completely absorbed by the sNECC. Consequently, it is difficult to compute the NECC transport without the NEUC influence.

In spite of their proximity, the forces that drive these two currents are likely to be different. As shown below, the NECC is directly wind-driven whereas it has been proposed that the NEUC is driven by the Eliassen–Palm flux of the tropical instability waves (Jochum and Malanotte-Rizzoli, 2004).

Based on Fig. 2, the NECC transport is defined as the eastward transport between 3°N and 13°N; the sNECC and nNECC are north and south of 8°N, respectively (Table 1). Two different depth-integrated transports were estimated: the depth-integrated transport (surface to bottom); and, to assess the utility of a 1.5 layer model, the transport above the thermocline.

Sverdrup transports were estimated from wind stress alone, as discussed in Section 2. The zonal transport inside the Ekman layer is also computed directly from the wind ($\tau^y/\rho_0 f$). The geostrophic transport is then estimated as the difference between Sverdrup and Ekman transport (Table 1). Fig. 3 shows the seasonal cycle of the Sverdrup, Ekman and geostrophic transports.

From Table 1, the annual mean values for both model and Sverdrup transports are very similar: the total NECC transport of 10.7 Sv is 95% of the mean Sverdrup transport (11.3 Sv). However, the total transport above the thermocline is only 60% (6.6 Sv) of the Sverdrup transport between

Table 1
Meridional and vertical current limits and annual mean, minimum and maximum values of transport at 35°W

Current	sNECC			nNECC			NECC		
Meridional limit	3–8°N			8–13°N			3–13°N		
Transport	Mean	Min	Max	Mean	Min	Max	Mean	Min	Max
Surface–thermocline	6.3	−3.2	15.2	0.3	−2.0	3.9	6.6	−5.2	17.0
surface–bottom	10.2	−1.8	17.4	0.5	−5.5	10.5	10.7	−1.8	22.2
Sverdrup	10.5	2.9	16.9	0.7	−3.3	10.3	11.3	1.4	24.1
Ekman	−0.5	−3.3	2.3	−1.1	−1.9	−0.1	−1.7	−5.3	2.2
Geostrophic (Sv–Ek)	11.1	6.0	16.8	1.9	−2.0	10.5	13.0	6.7	21.9

Transports are in Sverdrups.

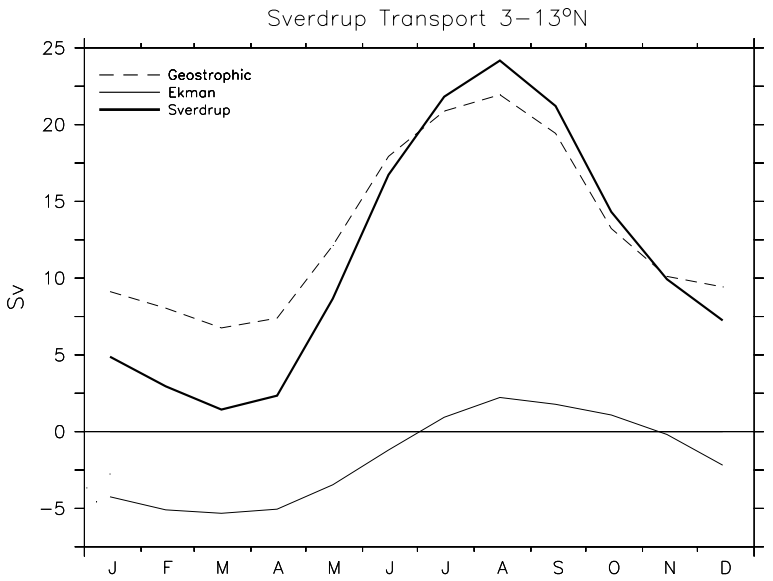

Fig. 3. Seasonal cycle of Sverdrup, Ekman and geostrophic transports at 35°W.

3°N and 13°N. This suggests that a 1.5-layer model, while useful for a qualitative description of the dynamics of the region, may be misleading for quantitative studies (see also Richardson and Reverdin (1987), Verdy and Jochum (2005)).

Fig. 4, which compares the seasonal cycles, shows that the Sverdrup balance explains the transports in the northern and southern part of the NECC but with a time-lag of about one month. This lag is most evident during the NECC intensification and decay. Interestingly, Fig. 4(d), which

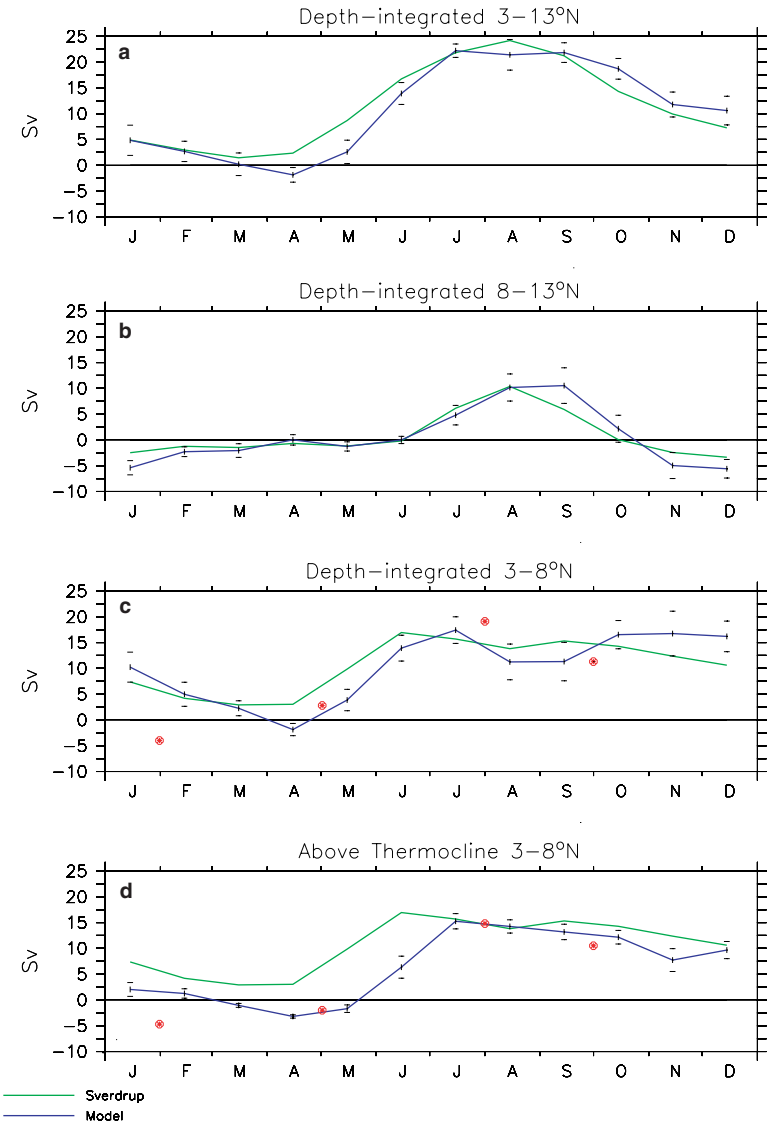

Fig. 4. Seasonal cycle of Sverdrup and model transports at 35°W for the NECC region (a), and for the nNECC and sNECC cores, (b) and (c) respectively. Horizontal bars in each month show the standard deviation based on a 4-year segment of the model output. The symbols correspond to the observed ADCP transports in the upper 400 m (c) and upper 150 m (d).

compares the Sverdrup transport with the transport above the thermocline, suggests a two-month time-lag, rather than a one-month time-lag.

An analysis of the stratification (not shown) demonstrates that the NECC response to the seasonal changes in the wind field is dominated by the first baroclinic mode. Using the long wave approximation and a first baroclinic Rossby radius $\lambda_1 = 178$ km (the model values are consistent with the observations of Emery et al. (1984)), the phase speed c was found to be -73 cm s^{-1}. Since the distance between 35°W and the African coast at the latitude of the NECC is approximately 2000 km, the transport of the NECC should lag the Sverdrup transport at 35°W approximately one month (see, however, Killworth and Blundell (2004) for a recent discussion of deviations from linear theory). This one-month time-lag is exactly what is found in the present study (Fig. 4(a)).

It is worth pointing out that considering only the NECC transport above the thermocline leads to an overestimation of the time-lag (compare Fig. 4(c) and (d)). The time-lag is most apparent in spring when the wind stress curl and the transport increase sharply. Since the transport above the thermocline is only a part of the Sverdrup transport, its graph is lower in the figure than the graph of the full transport. However, a similar position of the graph for the thermocline transport could also be achieved by moving the graph of the full transport to the right. Thus, the difference between the NECC transport and Sverdrup transport could be due to a time-lag or due an underestimation of the transport. In the present model we know the full NECC transport, and can therefore infer that the apparently increased time-lag in Fig. 4(d) is because there only part of the transport is captured. If thermocline transport observations, however, are interpreted as the full transport one would be mislead into thinking that there is two-month time-lag between the Sverdrup values and the NECC transport.

The time-lag found here is consistent with observations: Fonseca et al. (2004), through a combination of altimeter data, sea height anomaly, and hydrographic data, found a one-month lag between the positions of the ITCZ and the NECC (averaged between 30°W and 45°W). However, they also found that the maximum of wind stress curl and the NECC transport were separated by a time-lag of three months. Garzoli and Katz (1983) reported a one to two month phase lag between the wind stress curl and the thermocline depth between 42°W and 22°W. In both the studies uncertainties in the data lead to uncertainties in the estimated time-lag.

As there were only four expeditions instead of monthly ADCP measurements, a full seasonal cycle of transport cannot be presented. However, snapshots of the transport for the region between 3°N and 7.5°N, corresponding to the sNECC region, could be computed from ADCP observations and are summarized in Table 2. These values also were overlaid on the model

Table 2
Comparison between observations (ADCP) and model depth-integrated transports, in Sverdrups

Cruises	Season	Depth (m)			
		150		400	
		Data	Model	Data	Model
CITHER1	Winter	−4.7	3.3	−4.0	7.9
ETAMBOT2	Spring	−2.0	−1.6	2.8	1.8
EQUALANT99	Summer	14.8	15.3	19.1	19.8
ETAMBOT1	Fall	10.5	12.1	11.3	11.6

The integration limits are from sea-surface to 150 m and to 400 m, from 3°N to 7.5°N.

transport seasonal cycle (Fig. 4(c) and (d)). As the northernmost oceanographic station for all cruises was at 7.5°W, the transport northward of this latitude could not be estimated, and comparison for the nNECC region was not possible. To the best of our knowledge there are no other direct velocity measurements for the whole NECC region at 35°W. Echo-sounder arrays as described in Katz (1987), Garzoli and Richardson (1989) or Garzoli et al. (2004) do either not provide a sufficient meridional resolution or are too far west for the present purpose.

From Fig. 4 we conclude that, as in the other studies done with the present model (see Section 2), the forcing fields and the model setup are realistic enough to infer that the model dynamics is a representation of the ocean dynamics in the tropical Atlantic ocean, in particular at 35°W.

5. The two-core structure

To our knowledge the second core has never been observed directly. It is probably mentioned first in the modeling study of Schott and Böning (1991), but neither were its dynamics clear nor was it mentioned in any subsequent modeling studies. Inspired by the present model results we revisited historical observations to ensure that the second core is not only a model artifact.

Richardson and McKee (1984) studied the surface currents in the tropical Atlantic using historical ship-drift data. Zonal velocities computed from data grouped into one degree of latitude between 35°W and 45°W indicate the two maxima in the NECC structure. This feature is mostly evident during the second half of the year (Fig. 5), when the NECC appears at the surface. Even for the first half of the year, the two NECC cores are present and can be seen as the two adjacent minima in the westward surface flow. These minima are the signature of the two geostrophic subsurface eastward NECC cores. Richardson and Reverdin (1987) then analyzed surface drifter data and their Fig. 11 clearly shows two separate cores between 33°W and 23°W for March to May and for July to September. While these ship-drift and surface drifter data provide the strongest observational evidence for the two cores, other data indicate this second core as well.

Using a large number of hydrographic observations between 5°S and 20°N from the SECTIONS, WESTRAX, and FOCAL/SEQUAL programs, Chepurin and Carton (1997) described the climatological seasonal mass and geostrophic velocity fields. Maps with contours of geostrophic velocity clearly show the deep structure of the northern branch of the NECC during spring, summer and fall at 13°N (their Fig. 7). Bourlès et al. (1999b) show direct observations of velocity obtained with ADCPs, their September observation suggests an second core north of 7.5°N.

Didden and Schott (1992), through an intercomparison of Geosat altimetry and numerical model results, mention that the two-core structure appears in the seasonal current variations of both model and satellite data. However, no dynamical explanation was attempted.

It was shown here that both cores are in Sverdrup balance, therefore they must be generated by the particular structure of the wind field. It was also shown that the model results compare well with the observations and that in the observations the NECC has two cores as well. Therefore the observed wind field should predict the two cores, too. This is indeed the case (Fig. 6). From January to May the two cores are separated by a wedge of eastward flow, in June the second core moves as far north as 14°N and has a maximum transport in September.

Since we find the two NECC cores by using Sverdrup theory and wind field alone, it appears that we would not have needed the model in the first place. However, the very fact that almost

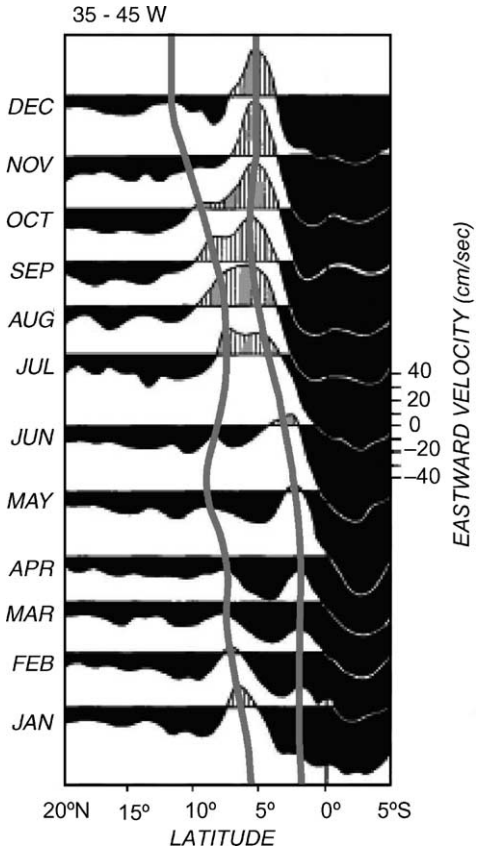

Fig. 5. Monthly north–south profiles of zonal velocity near the coast of Brazil at 35–45°W. Velocity values were computed from data grouped into 1°latitude × 10°longitude boxes. Gray lines (added by the present authors) show the positions of both, the nNECC and sNECC core. Adapted from Richardson and McKee (1984).

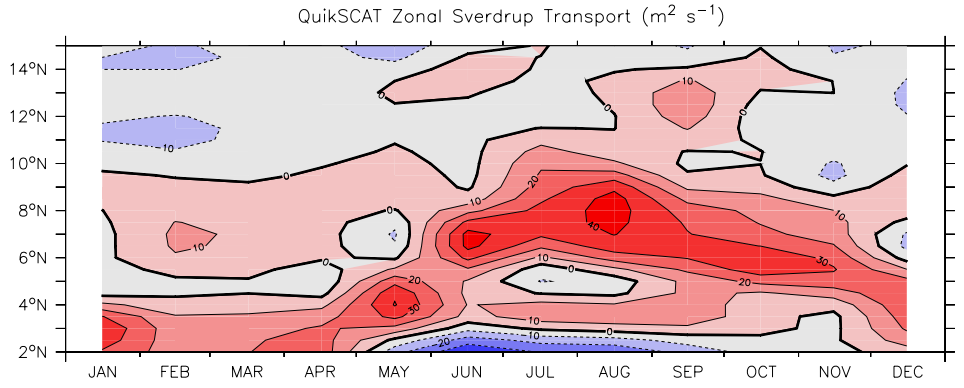

Fig. 6. Sverdrup transport at 35°W based on a 5 year climatology from QuikSCAT winds. Notice the two eastward cores that follow each other in a distance of approximately 4°. The latitudinal position of both cores has a seasonal range of approximately 6°.

all studies of the NECC that show two cores do not mention the second core suggests otherwise. The model is needed to provide a fresh perspective. In the model, the regular and smooth wind field makes the second core so obvious that it is hard to ignore or to interpret as random 'wiggle'.

The two maxima in the Sverdrup transport require two discrete maxima of the meridional derivative of the wind stress curl Eq. (6), one for each core. These maxima are located at the edges of the ITCZ, within the ITCZ the winds are weak and do not have strong gradients. Fig. 7 shows that approximately between 7°N and 12°N the wind stress is very weak, but pole and equatorward of this region the wind stress increases rapidly. The curl field is dominated by the meridional derivative of the zonal wind so that for the sake of simplicity we can assume that the transport associated with the NECC is proportional to the second meridional derivative of the zonal wind stress (τ^x_{yy}). Fig. 8 then illustrates the reason behind the NECC two-core structure: it is the reaction of

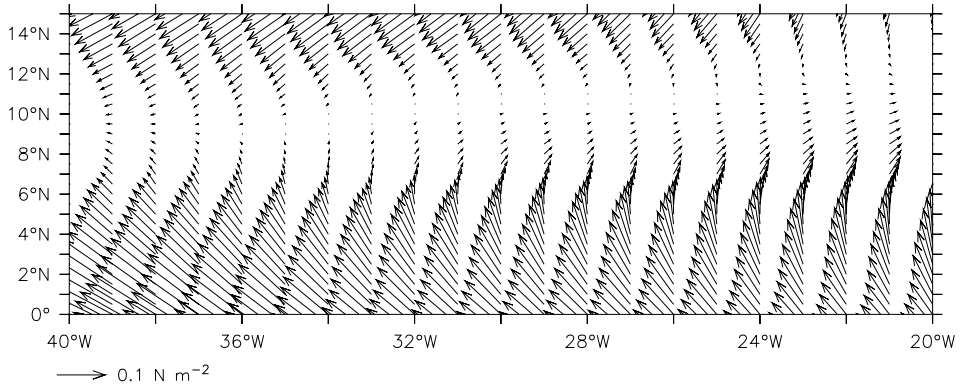

Fig. 7. Climatological wind-field for September, based on QuikSCAT. Note the spatial extent of the doldrums.

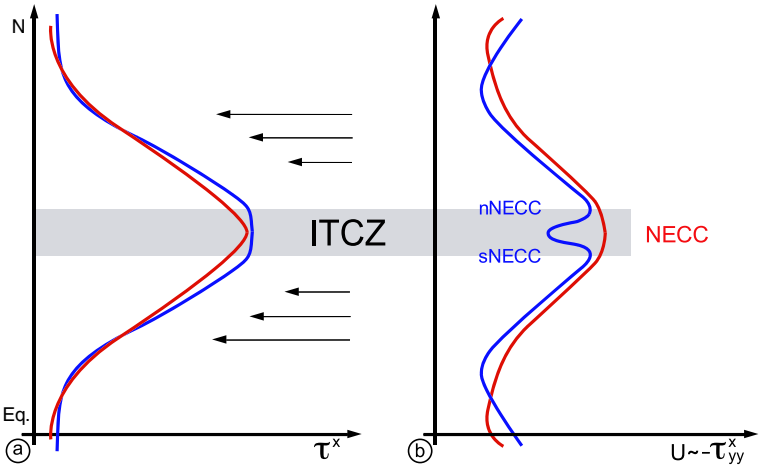

Fig. 8. Schematic diagram of (a) the zonal wind stress in two different situations: when the ITCZ is narrow and the inflection of τ^x is a sharp peak (red curve) and when the ITCZ is a broad area of constant τ^x generating a plateau shape (blue curve). (b) corresponds to the second y-derivative of each τ^x in (a), which according to the Sverdrup theory, is proportional to the zonal transport (U). The ITCZ is shown in gray. (For interpretation of the references in colour in this figure legend, the reader is referred to the web version of this article.)

the finite width of the ITCZ. If the ITCZ is a line crossing the basin, the curvature of the zonal wind stress has only one maximum which creates one NECC core. An ITCZ with a finite width has two curvature maxima, one at the northern and one at the southern end, which leads to two cores. The distance between the two cores is then set by the width of the ITCZ.

6. Summary

Theory, observations and a numerical model were used to understand the spatial and temporal structure of the NECC at 35°W.

The Sverdrup zonal transport was estimated and compared to the depth-integrated zonal transport obtained from model velocities. The annual mean model transport over the whole NECC region, 3–13°N, is 95% of the Sverdrup transport.

Consistent with observations, the seasonal cycle of the NECC transport lags the value predicted by Sverdrup approximately one month. For observational campaigns it is important to note that the model suggests that the transport above the thermocline underestimates the total NECC transport by approximately 40%. Hence, using the thermocline as lower boundary will overestimate the time-lag between NECC transport and its Sverdrup prediction.

It was shown that the NECC has two separate cores due to the particular wind-field generated by the Atlantic ITCZ. The zonal transport of the NECC at 35°W is mainly a function of the curvature of the zonal wind stress; hence, a finite-width ITCZ, which has two curvature maxima, produces two NECC cores.

Two cores have been mentioned before, first by Schott and Böning (1991) and then by Didden and Schott (1992). However, an explanation has never been given and the issue has not been discussed since. This is unfortunate, especially since the NECC is the classic textbook example for the explanatory power of the Sverdrup balance and a central feature of the tropical Atlantic circulation.

It is not surprising, however, when one keeps in mind that this double core structure is a feature of the Atlantic NECC only and there is only a limited set of observations beyond 5°N in the Atlantic. The authors could not find any evidence for the double core structure in the Pacific (see Kessler et al. (2003) for a recent analysis). Because the Sverdrup transport is the result of a zonal integration, the ITCZ has to be aligned strictly zonally to produce a double core structure. This makes the present result very sensitive to the choice of the wind field that is used to force the ocean model. Therefore we recalculated the zonal transport based on the Sverdrup balance with QuikSCAT winds: it also shows the double core structure for most of the year (Fig. 6). The most important piece of evidence, however, comes from ship-drift observations (Fig. 5). In spite of their coarse resolution they provide ample evidence for the existence of the double core NECC; the model in the present study was only used to understand the dynamics behind it.

Acknowledgements

We are grateful to Bernard Bourlès for providing the ADCP measurements and to Philip Richardson for insightful discussions. The QuikSCAT data is obtained from the NASA/NOAA

sponsored data system Seaflux, at JPL through the courtesy of W. Timothy Liu and Wenqing Tang, and with help of Olga T. Sato. This paper was written while the first author was a visiting student at the Department of Earth, Atmospheric and Planetary Sciences at MIT. Paola Malanotte-Rizzoli arranged for the visit and the CAPES Foundation provided funds. Markus Jochum was supported with NOAA grant NA16GP1576 and NASA grant NAG5-7194.

References

Arhan, M., Mercier, H., Bourlès, B., Gouriou, Y., 1998. Hydrographic sections across the Atlantic at 7°30N and 4°30S. Deep-Sea Res. I 45, 829–872.

Bourlès, B., D'Orgeville, M., Eldin, G., Gouriou, Y., Chucla, R., DuPenhoat, Y., Arnault, S., 2002. On the evolution of the thermocline and subthermocline eastward currents in the equatorial Atlantic. Geophys. Res. Lett. 29 (16), 1785.

Bourlès, B., Gouriou, Y., Chuchla, R., 1999a. On the circulation in the upper layer of the western equatorial Atlantic. J. Geophys. Res. C 104 (9), 21, 151–170.

Bourlès, B., Molinari, R.L., Johns, E., Wilson, W.D., Leaman, K.D., 1999b. Upper layer currents in the western tropical North Atlantic (1989–1991). J. Phys. Oceanogr. C 104 (1), 1361–1375.

Chepurin, G., Carton, J.A., 1997. The hydrography and circulation of the upper 1200 meters in the tropical North Atlantic during 1982–91. J. Mar. Res. 55, 633–670.

Didden, N., Schott, F., 1992. Seasonal variations in the Western Tropical Atlantic: surface circulation from geosat altimetry and woce model results. J. Geophys. Res. C 97 (3), 3529–3541.

Emery, W.J., Lee, W.G., Magaard, L., 1984. Geographic and seasonal distributions of Brunt–Väisälä frequency and rossby radii in the North Pacific and North Atlantic. J. Phys. Oceanogr. 14, 294–317.

Fonseca, C.A., Goni, G.J., Johns, W.E., Campos, E.J.D., 2004. Investigation of the North Brazil current retroaction and north equatorial countercurrent variability. Geophys. Res. Lett., 31. doi:10.1029/2004GL020901.

Garzoli, S., 1992. The Atlantic North Equatorial Countercurrent-models and observations. J. Geophys. Res. 97, 17931–17946.

Garzoli, S., Katz, E., 1983. The forced annual reversal of the Atlantic North Equatorial Countercurrent. J. Phys. Oceanogr. 13, 2082–2090.

Garzoli, S., Richardson, P., 1989. Low-frequency meandering of the Atlantic North Equatorial Countercurrent. J. Geophys. Res. 94, 2079–2090.

Garzoli, S., Ffield, A., Johns, W.E., Yao, Q., 2004. North Brazil current retroflection and transports. J. Geophys. Res., 109 (art. no. C01013).

Hellerman, S., Rosenstein, M., 1983. Normal monthly wind stress over the world ocean with error estimates. J. Phys. Oceanogr. 13, 1093–1104.

Jochum, M., Malanotte-Rizzoli, P., 2003. On the generation of North Brazil current rings. J. Mar. Res. 61 (2), 147–162.

Jochum, M., Malanotte-Rizzoli, P., 2004. A new theory for the generation of equatorial subsurface countercurrents. J. Phys. Oceanogr. 34, 755–771.

Jochum, M., Malanotte-Rizzoli, P., Busalacchi, A., 2004. Tropical instability waves in the Atlantic Ocean. Ocean Modell. 7 (1–2), 145–163.

Katz, E.J., 1987. Seasonal response of the sea surface to the wind in the equatorial Atlantic. J. Geophys. Res. 92, 1885–1893.

Katz, E.J., Garzoli, S., 1982. Response of the western equatorial Atlantic Ocean to an annual wind cycle. J. Mar. Res. 40, 307–329.

Kessler, W., Johnson, G., Moore, D., 2003. Sverdrup and nonlinear dynamics of the pacific equatorial currents. J. Phys. Oceanogr. 33, 994–1008.

Killworth, P.D., Blundell, J.R., 2004. The dispersion relation for planetary waves in the presence of mean flow and topography. Part I: Analytical theory and one-dimensional examples. J. Phys. Oceanogr. 34, 2692–2711.

Large, W.G., Pond, S., 1981. Open ocean momentum flux measurements in moderate to strong winds. J. Phys. Oceanogr. 11, 324–336.

Liu, W.T., 2002. Progress in scatterometer application. J. Oceanogr. 58, 121–136.
Liu, Z., Philander, S., 1995. How different wind stress patterns affect the tropical–subtropical circulations of the upper ocean. J. Phys. Oceanogr. 25, 449–462.
Richardson, P., Reverdin, G., 1987. Seasonal cycle of velocity in the Atlantic NECC as measured by surface drifters, current meters and ship drifts. J. Geophys. Res. 92, 3691–3708.
Richardson, P.L., McKee, T.K., 1984. Average seasonal variation of the Atlantic Equatorial Currents from historical ship drifts. J. Phys. Oceanogr. 14, 1226–1238.
Schott, F.A., Böning, C.W., 1991. The woce model in the Western Equatorial Atlantic: upper layer circulation. J. Geophys. Res. C 96 (4), 6993–7004.
Schott, F.A., Fischer, J., Stramma, L., 1998. Transports and pathways of the upper-layer circulation in the Western Tropical Atlantic. J. Phys. Oceanogr. 28, 1904–1928.
Sverdrup, H., 1947. Wind-driven currents in a baroclinic ocean, with application to the equatorial currents in the eastern Pacific. Proc. Nat. Acad. Sci., USA 33, 318–326.
Verdy, A., Jochum, M., 2005. A note on the validity of the Sverdrup balance in the Atlantic North Equatorial Countercurrent. Deep–Sea Res. I 52 (1), 179–188.